

Phase diagram of thin films of lutetium hydride—lutetium

Haofeng Chen(陈浩锋), Xin Yang(杨鑫), and Lixin Cao(曹立新)
Citation: Chin. Phys. B, 2026, 35 (**5**): 057303. DOI: 10.1088/1674-1056/ae48c7
http://cpb.iphy.ac.cn; http://iopscience.iop.org/cpb

What follows is a list of articles you may be interested in

Electron doping in FeSe monolayer and multilayer via metal phthalocyanine adsorption: A first-principles investigation

Fangyu Yang(杨方玉), Yan-Fang Zhang(张艳芳), Peixuan Li(李佩璇), and Shixuan Du(杜世萱)
Chin. Phys. B, 2025, 34 (**11**): 117302. DOI: 10.1088/1674-1056/ae0396

Enhancing room-temperature thermoelectricity of $SrTiO_3$ based superlattices via epitaxial strain

Yi Zhu(朱怡), Hao Liu(刘昊), Huilin Lai(赖辉琳), Zhenghua An(安正华), Yinyan Zhu(朱银燕), Lifeng Yin(殷立峰), and Jian Shen(沈健)
Chin. Phys. B, 2025, 34 (**9**): 097305. DOI: 10.1088/1674-1056/ade24e

Quantum anomalous Hall effect in twisted bilayer graphene

Wen-Xiao Wang(王文晓), Yi-Wen Liu(刘亦文), and Lin He(何林)
Chin. Phys. B, 2025, 34 (**4**): 047301. DOI: 10.1088/1674-1056/adb38a

Electrochemical liftoff of freestanding GaN by a thick highly conductive sacrificial layer grown by HVPE

Xiao Wang(王骁), Yu-Min Zhang(张育民), Yu Xu(徐俞), Zhi-Wei Si(司志伟), Ke Xu(徐科), Jian-Feng Wang(王建峰), and Bing Cao(曹冰)
Chin. Phys. B, 2021, 30 (**6**): 067306. DOI: 10.1088/1674-1056/abd6fa

First-principles study of non-radiative carrier capture by defects at amorphous-SiO_2/Si(100) interface

Haoran Zhu(祝浩然), Weifeng Xie(谢伟锋), Xin Liu(刘欣), Yang Liu(刘杨), Jinli Zhang(张金利), and Xu Zuo(左旭)
Chin. Phys. B, 2023, 32 (**7**): 077303. DOI: 10.1088/1674-1056/ac9fc2

Phase diagram of thin films of lutetium hydride — lutetium

Haofeng Chen(陈浩锋)[1,2,†], Xin Yang(杨鑫)[1,2,†], and Lixin Cao(曹立新)[1,2,‡]

[1] *Beijing National Laboratory for Condensed Matter Physics, Institute of Physics, Chinese Academy of Sciences, Beijing* 100190, *China*
[2] *University of Chinese Academy of Sciences, Beijing* 100190, *China*

(Received 12 January 2026; revised manuscript received 13 February 2026; accepted manuscript online 23 February 2026)

Lutetium hydrides LuH_x thin films with x from 0 up to 3.2 were deposited on Si(001) substrates by laser ablating a 4N lutetium metal target in a vacuum or hydrogen environment. With x increasing, the hydride films undergo a phase transition at $x \sim 0.77$ from hexagonal close-packed (hcp) to face-centered cubic (fcc) structures. The anomaly was found to emerge in temperature-dependent resistivity at ~ 173 K in hcp-phase films but not in fcc-phase films. The sudden dramatic decrease in the amplitude of the anomaly once hydride enters the two-phase region from the hcp-phase side supports the idea that the formation of the hydrogen network in the *a*–*b* plane of the hcp-phase is the sole reason for the emergence of the anomaly.

Keywords: lutetium, hydride, thin film, heavy rare earth metal

PACS: 73.61.At, 68.55.Nq, 71.20.Eh

DOI: 10.1088/1674-1056/ae48c7 **CSTR:** 32038.14.CPB.ae48c7

1. Introduction

Stirred by an assertion claiming room-temperature superconductivity under "near-ambient" pressure in nitrogen-doped lutetium hydrides, hydrides of lutetium LuH_x suddenly attracted booming attention, much of it focused on bulk materials synthesized and investigated under high pressure.[1–6] Thorough examinations of the original assertion led to a retraction; however, the follow-up works did initiate a new wave of research on the hydrides of lutetium, most of which are under high pressure. Prior to this wave of studies, precedent studies under ambient pressure had revealed a hydrogen-dependent anomaly at around 170 K in resistivity,[7–9] which was further linked to the formation of low-dimensional ordering of hydrogen/deuterium atoms inside the crystals.[8,10–12] Similar resistivity anomalies under ambient pressure are universal in ferromagnetic heavy rare earth metals (Gd, Tb, Dy, Ho, Er, and Tm);[13–22] however, the resistivity anomaly in lutetium hydride crystals was not magnetically related.[22–25] We noticed that some experimental findings under ambient pressure were not observed in the recent experiments on high or "near-ambient" pressure, e.g., the hydrogen-dependent anomaly at around 170 K in the resistivity of lutetium hydride crystals. Therefore, in order to systematically understand lutetium hydride in a wider range, it is intriguing to study another physical form, if possible: thin films of lutetium hydride in this paper, as knowledge of them is rare up to now. Such a study may shed some light on a comprehensive understanding of lutetium hydride.

In this paper, we present deposition and systematic characterizations of lutetium hydride LuH_x thin films. The hydrogen concentration x can be boosted as high as 3.2 in the nominal formula, i.e., $LuH_{3.2}$, at which its crystal structure still persists in face-centered cubic (fcc). With x increasing, the films undergo a structural phase transition at $x \sim 0.77$ from hexagonal close-packed (hcp) to fcc structures. The temperature-dependent anomalies of resistivity at ~ 173 K were observed at ambient pressure, which is observed in the lutetium hydride thin films for the first time experimentally.

2. Experimental details

Over 420 lutetium hydride films were synthesized by pulsed laser deposition (PLD) with a vacuum chamber base pressure of 6.0×10^{-7} Pa. A KrF excimer laser of 248-nm wavelength and 5-Hz repetition rate was irradiated on a 99.99% lutetium ingot (Grirem Advanced Materials) that was 15 mm in diameter and 8 mm in height, under either vacuum pumping or a flowing hydrogen environment maintained at certain pressures. An Si(001) substrate was placed 20 mm away from the 65-mJ/mm^2 laser beam impinging on the ingot surface and was heated to 420 °C for film deposition.

PLD chamber is part of an *in-situ* thin film deposition and characterization complete equipment, which consists of individual equipment for the PLD, x-ray diffraction (XRD), sputtering metallization, ultrasonic welding, and low-temperature transport measurement down to 2 K, etc. Each individual equipment is settled inside a glove box which is a confined space filled with ambient-pressure nitrogen or inert gas argon in order to significantly reduce the possible contamination

† These authors contributed equally to this work.
‡Corresponding author. E-mail: lxcao@iphy.ac.cn

© 2026 Chinese Physical Society and IOP Publishing Ltd. All rights, including for text and data mining, AI training, and similar technologies, are reserved.

from oxygen and moisture in the air. The levels of impurity from oxygen and water molecules are limited and maintained below ~ 0.1 ppm. All the individual equipment is connected to each other through a transfer mechanism which is also confined and filled with ambient-pressure nitrogen or argon.

Some film samples were characterized *ex-situ* by ULVAC-PHI nano TOF II for time-of-flight — secondary ion mass spectrometry (TOF-SIMS). Film thickness was measured on a Dektak stylus profilometer. The samples were stored in vacuum-desiccators temporarily and thus transferred between laboratories.

3. Results and discussion

The XRD spectra of a set of films deposited from a vacuum up to a hydrogen pressure of 2 Pa are displayed in Figs. 1(a)–1(m). The film thicknesses measured via step edges are ~ 500 nm. Obviously, the films are thick enough to be strain-relaxed and therefore polycrystalline, which, in comparison with the thinner, epitaxial, single-oriented films, makes it easier to study the crystalline structure of a not well-known film material using XRD.

A crystallographic phase transition can be seen clearly: (i) pure hcp-phase when hydrogen pressure $[H_2] \leq 1.6 \times 10^{-4}$ Pa, (ii) hcp- and fcc-phases coexistence when 1.6×10^{-4} Pa $< [H_2] < 1.0 \times 10^{-3}$ Pa, (iii) pure fcc-phase when $[H_2] \geq 1.0 \times 10^{-3}$ Pa. Note that the phase boundary between the hcp one-phase region and the hcp/fcc two-phase region is somewhere in the range of 1.6×10^{-4} Pa $< [H_2] < 2.0 \times 10^{-4}$ Pa. Deduced from Fig. 1, the lattice constants of the hcp-phase or fcc-phase as a function of hydrogen pressure are plotted in Fig. 2(a).

In order to understand the hydriding process meticulously, a TOF-SIMS experiment was performed on another set of film samples, the deposition parameters of which are the same as those shown in Fig. 1, except that the deposition time is one-third of the latter. Ar^+ ion beam was used to sputter exfoliating the film into dimple of certain depth, while $Bi_3{}^{++}$ cluster beam was used to bombard secondary ions/clusters out for mass-charge ratio analysis. The concentration depth profile of a hydride film deposited at 1.0×10^{-4} Pa is plotted in Fig. 2(b). It is worthy to note that the dominant detected substances are univalent ions or clusters, while no evident high valence ions or clusters were found in the SIMS experiment although lutetium is a trivalent metal.

Further effort has to be made since the SIMS experimental result gives only the relative content ratios among the elements measured. Therefore, we fine-tuned the deposition pressure and captured a phase point that is at the boundary between the hcp/fcc two-phase region and the fcc single-phase region. The hydrogen content x of the film right at the phase boundary is thus calibrated as 1.8.[26] Note: (i) the solution concentrations of hydrogen in the fcc-phases at different phase points in the hcp/fcc two-phase region are all the same, while those in the fcc single-phase region are not; (ii) the lattice constants of fcc-phases right at the phase boundary and in the hcp/fcc two-phase region are equal to each other, while those at the phase boundary and in the fcc single-phase region are not.

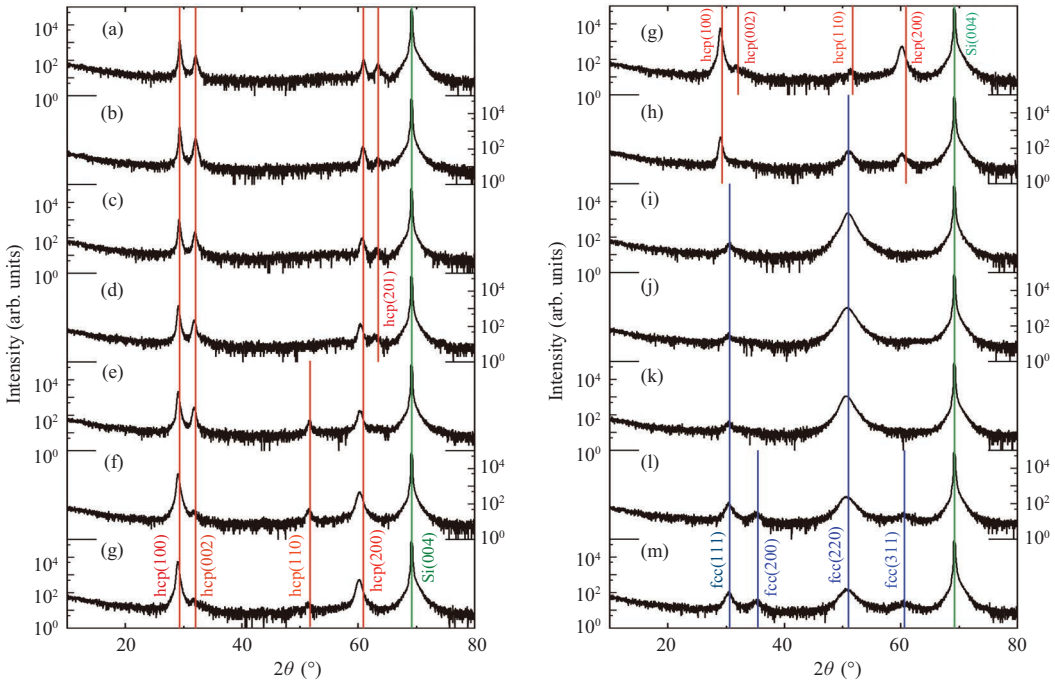


Fig. 1. XRD spectra of films deposited at hydrogen pressures of 0 Pa, 4.0×10^{-6} Pa, 1.0×10^{-5} Pa, 5.0×10^{-5} Pa, 1.0×10^{-4} Pa, 1.2×10^{-4} Pa, 1.6×10^{-4} Pa, 2.0×10^{-4} Pa, 1.0×10^{-3} Pa, 5.0×10^{-3} Pa, 1.0×10^{-2} Pa, 1.0×10^{-1} Pa, and 2.0×10^{0} Pa, respectively. Perpendicular red, blue, and green lines are guides to the eye for the diffraction peaks of hcp lutetium hydride, fcc lutetium hydride, and Si(004), respectively.

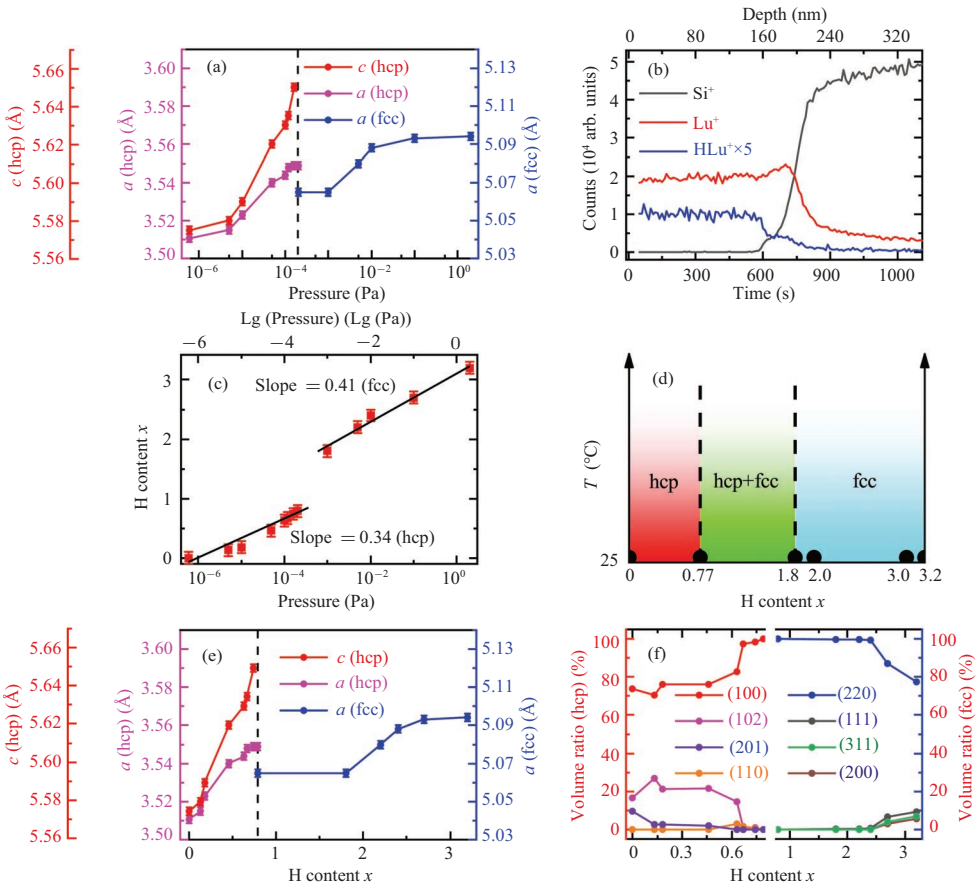


Fig. 2. (a) Lattice constants of hcp- and fcc-phases as a function of hydrogen pressure during deposition; (b) SIMS depth profiles of Si^+ ions, Lu^+ ions, and HLu^+ clusters, respectively; the counts of HLu^+ clusters were magnified by a factor of 5; (c) hydrogen content of the film as a function of hydrogen pressure during deposition; (d) Lu–LuH_x ($x = 3.2$) phase diagram; (e) lattice constants of hcp- and fcc-phases as a function of hydrogen content; (f) hydrogen content-dependent relative volume ratio of grains of each type of preferred orientation.

Corresponding to the XRD result shown in Fig. 2(a) and the analysis performed above, the phase boundary between the hcp one-phase region and the hcp/fcc two-phase region is somewhere between 1.6×10^{-4} Pa $< [H_2] < 2.0 \times 10^{-4}$ Pa, which means $0.74 < x < 0.79$ in terms of hydrogen content in the film, roughly at $x \sim 0.77$.

Moreover, the calibrated relationship between hydrogen content and deposition pressure is given in Fig. 2(c). It can be seen that the hydrogen concentration x follows different semi-logarithmic functions along with hydrogen pressure during deposition: (i) lower than 2.0×10^{-4} Pa, the data fit a line with a slope of 0.34/lg(Pa); (ii) higher than 1.0×10^{-3} Pa, the data fit another line with a slope of 0.41/lg(Pa). This should be the case if one takes the phase transition and therefore the formation of two different kinds of solid-state phases into account. Note that the formation of different solid-state phases means different chemical reaction processes, including thermodynamics, solution and solubility in solid-state compounds, diffusion processes, and reaction dynamics, etc.

The phase relationship thus determined is summarized in Fig. 2(d) as a phase diagram. It is interesting to note that in our films, (i) the fcc single-phase region persists with x from 1.8 up to 3.2; (ii) LuH_3 possesses an fcc structure, rather than a trigonal structure with space group $P\bar{3}c1$,[27–31] which is common for bulk materials synthesized under pressure; (iii) the hcp single-phase region persists with x from 0 up to 0.77; (iv) the hcp-phase and fcc-phase coexist in the two-phase region with x from 0.77 to 1.8.

From the above experiments and analyses, it is clear that the hydriding process can be controlled in a precise way by manipulating the technical parameter of hydrogen pressure. Figure 2(a) is replotted in Fig. 2(e), in which the lattice constants as a function of hydrogen content, instead of pressure, are shown. Moreover, the percentage ratios of the volume of grains of each individual crystalline orientation can be calculated based on the integrated intensities of diffractions in the films and from the literature,[32,33] with the final results given in Fig. 2(f). It can be seen that the preferred orientations are (100) and (220) for hcp- and fcc-phases, respectively.

Epitaxy relationships between the substrate and films are attempted to be exhaustively searched, given as shown in Figs. 3 and 4 for hcp- and fcc-phases, respectively, for all possible geometrical matching possibilities of the lattices of the film and substrate at the interface. Accordingly, the parameters are summarized in Tables 1 and 2.

Table 1. Calculated lattice mismatches and percentages of unoccupied lattice points for possible epitaxial mechanisms illustrated in Fig. 3 by the ball-and-stick models for hcp-phase LuH_x film epitaxy.

$LuH_x(hkl)$	Illustration	Lattice mismatch		Unoccupied	Unoccupied	$LuH_x(hkl)$	Illustration	Lattice mismatch		Unoccupied	Unoccupied
		x_1 (0 °)	y_1 (90 °)	point Lu	point Si			x_2 (45 °)	y_2 (135 °)	point Lu	point Si
(100)	Fig. 3(a)	8.4%	–9.0%	66.7%	75.0%	(100)	Fig. 3(b)	–2.7%	2.9%	66.7%	75.0%
(002)	Fig. 3(c)	8.4%	–5.7%	75.0%	66.7%	(002)	Fig. 3(d)	–12.2%	2.9%	83.3%	75.0%
(201)	Fig. 3(e)	8.4%	–0.4%	50.0%	83.3%	(201)	Fig. 3(f)	2.9%	–6.5%	66.7%	87.5%
(110)	Fig. 3(g)	–5.8%	3.1%	87.5%	88.9%	(110)	Fig. 3(h)	–12.2%	–2.7%	50.0%	50.0%

Table 2. Calculated lattice mismatches and percentages of unoccupied lattice points for possible epitaxial mechanisms illustrated in Fig. 4 by the ball-and-stick models for fcc-phase LuH_x film epitaxy.

$LuH_x(hkl)$	Illustration	Lattice mismatch		Unoccupied	Unoccupied	$LuH_x(hkl)$	Illustration	Lattice mismatch		Unoccupied	Unoccupied
		x_1(0 °)	y_1(90 °)	point Lu	point Si			x_2(45 °)	y_2(135 °)	point Lu	point Si
(220)	Fig. 4(a)	7.3%	1.7%	66.7%	75.0%	(220)	Fig. 4(b)	7.3%	1.7%	66.7%	75.0%
(111)	Fig. 4(c)	7.3%	−7.0%	75.0%	66.7%	(111)	Fig. 4(d)	−13.5%	1.7%	83.3%	75.0%
(311)	Fig. 4(e)	7.3%	–2.4%	50.0%	66.7%	(311)	Fig. 4(f)	1.7%	−8.7%	66.7%	75.0%
(200)	Fig. 4(g)	1.7%	1.7%	88.9%	93.75%	(200)	Fig. 4(h)	7.3%	7.3%	0.0%	50.0%

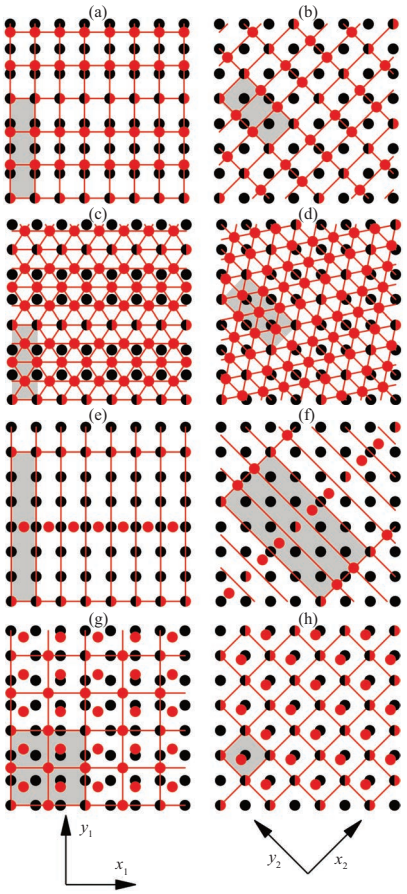


Fig. 3. Schematic ball-and-stick models for hcp-phase LuH_x ($x \leq 0.79$) epitaxy on Si(001). The black balls are Si ions of the Si(001) plane at the interface, while the red balls and sticks represent Lu ions and LuH_x lattices, respectively. The shaded greyish block marks the unit cells of the substrate and film matched to each other. The lattice points at the corners of the cells are illustrated as reddish-black dots. Note that hcp- and fcc-phases coexist in $LuH_{0.79}$.

For the hcp-phase, the (100)-oriented film indeed shows the smallest lattice mismatch as illustrated in Fig. 3(b). For the fcc-phase, the situation becomes a bit complicated. The final winner, the (220)-orientation as illustrated in Figs. 4(a) and 4(b), seems to be a compromise between lattice mismatch and lattice point unoccupancy, the latter of which is a manifestation of how many or how few dangling bonds there are at the interface.

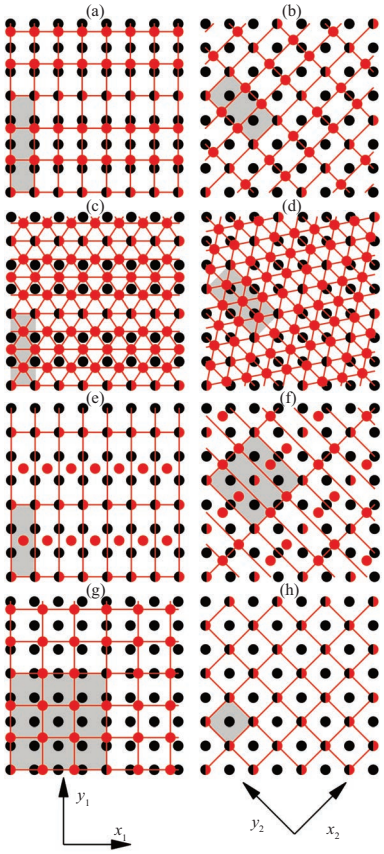


Fig. 4. Schematic ball-and-stick models for fcc-phase LuH_x ($x \geq 0.79$) epitaxy on Si(001). The black balls are Si ions of the Si(001) plane at the interface, while the red balls and sticks represent Lu ions and LuH_x lattices, respectively. The shaded greyish block marks the unit cells of the substrate and film matched to each other. The lattice points at the corners of the cells are illustrated as reddish-black dots. Note that fcc- and hcp-phases coexist in $LuH_{0.79}$.

The resistivities of a set of films of $\sim$ 500-nm thick LuH_x ($0 < x \leq 3.2$) were measured *in-situ* as a function of temperature, as shown in Fig. 5(a). First-order and second-order differentials of the curves shown in Fig. 5(a) are given in Figs. 5(b) and 5(c), respectively. A kink can be seen clearly at $\sim$ 173 K

for films with $x \leq 0.79$, i.e., $x = 0.09$, 0.13, 0.18, 0.46, 0.63, and 0.79. As shown in Figs. 5(b) and 5(c), the transition is quite broad, from $\sim$ 190 K down to $\sim$ 155 K.

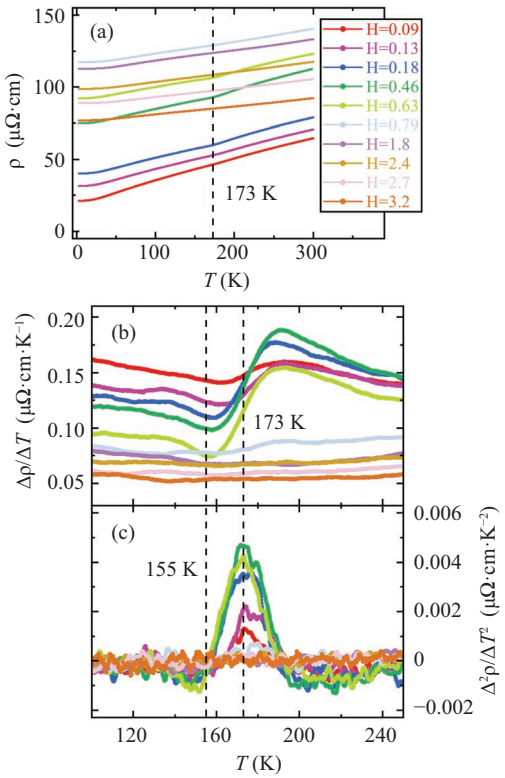


Fig. 5. Transport properties of lutetium hydride films: (a) temperature dependences of resistivities of 10 films with hydrogen content variation; (b) first order differential of plots given in panel (a); (c) second order differential of plots given in panel (a).

Note, (i) the resistivity kink at $x = 0.79$ is very weak, consistent with the coexistence of both hcp- and fcc-phases; (ii) the kink could not be observed in films with $x = 1.8$, 2.4, 2.7, and 3.2. The absence of the kink in the fcc-phase reinforces the fact that the anomaly is only associated with the hcp-phase, not with the fcc-phase LuH_x.

The phenomenon is the same as what had been found decades ago in bulk materials at ambient pressure.[7–12] This is the first time the transport property anomaly has been observed in the thin films of lutetium hydride. Since the transition is quite broad, it might be a second-order phase transition or even higher, rather than a first-order one.

Regarding the dramatic weakness of the resistivity anomaly for LuH_x with $x = 0.79$, which is in the hcp/fcc two-phase region, in comparison with the anomalies observed in the pure single hcp-phase, the low dimensionality of the thin film might be the reason. As the neutron scattering studies revealed that the deuterium correlated with each other to form a linear ordering within the *a*–*b* plane,[8,10–12] it is believed that the linear ordering of hydrogen is related to the resistivity anomaly.

Our experimental findings, the dramatic weakness of the resistivity anomaly in the thin film in the two-phase region, may further suggest that these ordered hydrogen networks in the *a*–*b* plane are the sole reason for the resistivity anomaly.

The reasons are: (i) for the hcp-phase LuH_x with $x < 0.77$, *c.f.*, Figs. 1(a)–1(g), the ordered hydrogen networks in the *a*–*b* plane of the films are intact, verified by the appearance of their (002) diffraction peaks of the hcp-phase; i.e., no matter whether the diffraction intensities are higher or lower, they can be observed, which means the volume ratios of the (001)-oriented hcp-phase grains in the $x < 0.77$ films are above the detection limit of the XRD, which might be around several percentage points or higher; (ii) for the hcp-phase LuH_x with $x = 0.79$, *c.f.*, Fig. 1(h), the (002) diffraction peak of the hcp-phase cannot be observed, which means the (001)-oriented hcp-phase grains are not detectable by the XRD and therefore their volume ratio is very low; (iii) in comparison to the thin film with the bulk crystal, the low dimensionality leads to the transport network being more easily broken in the former form of material than in the latter; (iv) the grains of the (100)-oriented hcp-phase, *c.f.* Fig. 1(h), do not help the emergence of the transport anomaly.

4. Conclusion

Employing a complete equipment comprising a PLD chamber, lutetium hydrides LuH_x thin films utilizing a 4N lutetium target were deposited and characterized meticulously. A two-phase region of hcp- and fcc-phases exists in between $0.77 < x < 1.8$. With $x < 0.77$, the LuH_x film is in the hcp-phase single-phase region, while with $x > 1.8$, it is in the fcc-phase single-phase region. The LuH_x film persists in the fcc-phase up to $x = 3.2$ corresponding to 2-Pa hydrogen pressure during deposition. The films are polycrystals, with (100) and (220) orientations being preferred for epitaxy for hcp- and fcc-phases, respectively.

The resistivity kink at $\sim$ 173 K, with the lower critical point at $\sim$ 155 K and the higher critical point at $\sim$ 190 K, was observed for the first time in the thin films of lutetium hydride. The kink anomaly was found to appear only in hcp-phase films but not in fcc-phase films. The sudden dramatic decrease in the amplitude of the anomaly once hydride enters the two-phase region from the hcp-phase side supports the idea that the formation of the hydrogen network in the *a*–*b* plane of the hcp-phase is the sole reason for the emergence of the anomaly.

Acknowledgment

Project supported by the National Key Research and Development Program of China (Grant Nos. 2023YFB3507303 and 2022YFF0706102).

References

[1] Ming X, Zhang Y J, Zhu X, Li Q, He C, Liu Y, Huang T, Liu G, Zheng B, Yang H, Sun J, Xi X and Wen H H 2023 *Nature* **620** 7972

[2] Zhang Y J, Ming X, Li Q, Zhu X, Zheng B, Liu Y, He C, Yang H and Wen H H 2023 *Sci. China: Phys. Mech. Astron.* **66** 287411

[3] Sha P, Wang N, Zheng X, Qiu Q, Peng Y and Cheng J 2023 *Chin. Phys. Lett.* **40** 046101

[4] Guo J, Cai S, Wang D, Shu H, Yang L, Wang P, Wang W, Tian H, Yang H, Zhou Y, Zhao J, Han J, Li J, Wu Q, Ding Y, Yang W, Xiang T, Mao H K and Sun L 2023 *Chin. Phys. Lett.* **40** 097401

[5] Li Z, He X, Zhang C, Lu K, Min B, Zhang J, Zhang S, Zhao J, Shi L, Peng Y, Feng S, Deng Z, Song J, Liu Q, Wang X, Yu R, Wang L, Li Y, Bass J D, Prakapenka V, Chariton S, Liu H and Jin C 2023 *Sci. China: Phys. Mech. Astron.* **66** 267411

[6] Wang D, Wang N, Zhang C, Xia C, Guo W, Yin X, Bu K, Nakagawa T, Zhang J, Gorelli F, Dalladay S P, Meier T, Lü X, Sun L, Cheng J, Zeng Q, Ding Y and Mao H K 2024 *Matter Radiat. Extremes* **9** 037401

[7] Daou J N, Lucasson A and Lucasson P 1976 *Solid State Commun.* **19** 895

[8] Vajda P, Daou J N, Burger J P, Kai K, Gschneidner Jr K A and Beaudry B J 1986 *Phys. Rev. B* **34** 5154

[9] Daou J N, Vajda P, Lucasson A, Lucasson P and Burger J P 1986 *Philos. Mag. A* **53** 611

[10] Blaschko O, Krexner G, Daou J N and Vajda P 1985 *Phys. Rev. Lett.* **55** 2876

[11] Blaschko O, Krexner G, Pleschiutschnig J, Ernst G, Daou J N and Vajda P 1989 *Phys. Rev. B* **39** 5605

[12] Pleschiutschnig J, Schwarz W, Blaschko O, Vajda P and Daou J N 1991 *Phys. Rev. B* **43** 5139

[13] Legvold S, Spedding F H, Barson F and Elliott J F 1953 *Rev. Mod. Phys.* **25** 129

[14] Nellis W J and Legvold S 1969 *Phys. Rev.* **180** 581

[15] Thoburn W C, Legvold S and Spedding F H 1958 *Phys. Rev.* **112** 56

[16] Elliott J F, Legvold S and Spedding F H 1954 *Phys. Rev.* **94** 1143

[17] Behrendt D R, Legvold S and Spedding F H 1958 *Phys. Rev.* **109** 1544

[18] Rhodes B L, Legvold S and Spedding F H 1958 *Phys. Rev.* **109** 1547

[19] Elliott J F, Legvold S and Spedding F H 1955 *Phys. Rev.* **100** 1595

[20] Green R W, Legvold S and Spedding F H 1961 *Phys. Rev.* **122** 827

[21] Edwards L R and Legvold S 1968 *Phys. Rev.* **176** 753

[22] Colvin R V, Legvold S and Spedding F H 1960 *Phys. Rev.* **120** 741

[23] Stierman R J and Gschneidner K A Jr 1984 *J. Magn. Magn. Mat.* **42** 309

[24] Spedding F H and Croat J J 1973 *J. Chem. Phys.* **59** 2451

[25] Lee R S and Legvold S 1967 *Phys. Rev.* **162** 431

[26] Daou J N and Bonnet J E 1974 *J. Phys. Chem. Solids* **35** 59

[27] Moulding O, Gallego P S, Gao Y, Toulemonde P, Garbarino G, De Rango P, Pairis S, Giroux P and Méasson M A 2023 *Phys. Rev. B* **108** 214545

[28] Peng Y A, Wang H Y, Su F H, Wang P, Xu H A, Liu L, Yu L X, Howie R T, Xu W, Gregoryanz E and Liu X D 2025 *Matter Radiat. Extremes* **10** 017804

[29] Li X, Wang Y, Fu Y, Redfern S A T, Jiang S, Zhu P and Cui T 2024 *Adv. Sci.* **11** 2401642

[30] Sun Y, Zhang F, Wu S, Antropov V and Ho K M 2023 *Phys. Rev. B* **108** L020101

[31] Palasyuk T and Tkacz M 2005 *Solid State Commun.* **133** 481

[32] I Liu L G 1975 *J. Phys. Chem. Solids* **36** 31 (CDD PDF-4 file 03-065-4096)

[33] Pebler A and Wallace W E 1962 *J. Phys. Chem.* **66** 148 (ICDD PDF-4 file 04-033-4751)